

Review

Review of the Thermoelectric Properties in Nanostructured Fe₂VAl

Eric Alleno

Institut de Chimie et des Matériaux Paris-Est, Université Paris-Est, UMR 7182 CNRS—UPEC, 2 rue H. Dunant, 94320 Thiais, France; eric.alleno@icmpe.cnrs.fr; Tel.: +33-1-4978-1237

Received: 4 October 2018; Accepted: 17 October 2018; Published: 24 October 2018



Abstract: Besides alloying, nanostructuring was implemented to improve the thermoelectric properties in Fe₂VAl. This Heusler alloy indeed displays a thermoelectric figure of merit too small for applications ($ZT \sim 0.1$ at 300 K) which is caused by a large lattice thermal conductivity ($\lambda_L = 27 \text{ W}\cdot\text{m}^{-1}\cdot\text{K}^{-1}$ at 300 K). The effect of nanostructuring on the microstructure and on the thermoelectric properties of alloyed Fe₂VAl are therefore reviewed. By mechanical alloying followed by spark plasma sintering, the average grain size (D) was decreased to $D \sim 300\text{--}400$ nm in Fe₂VAl_{0.9}Si_{0.1}, Fe₂VAl_{0.9}Si_{0.07}Sb_{0.03}, Fe₂V_{1.05}Al_{0.95}, and Fe₂V_{0.9}W_{0.1}Al. As expected, phonon scattering at the numerous grain boundaries lead to a strong decrease in the lattice thermal conductivity, which reached values as small as $\lambda_L = 3.3 \text{ W}\cdot\text{m}^{-1}\cdot\text{K}^{-1}$. However, in all the reviewed examples, the thermoelectric figure of merit (ZT) is only marginally or not even improved when comparing to non-nanostructured samples because the electrical resistivity also increases upon nanostructuring. A significantly improved $ZT = 0.3$ at 500 K was only recently observed in severely deformed Fe₂VAl_{0.95}Ta_{0.05} by high pressure torsion because the very fine microstructure ($D \sim 100$ nm) strongly enhanced the thermal conductivity reduction.

Keywords: thermoelectricity; Heusler alloys; thermal conductivity; electrical resistivity; grain boundaries; ball-milling; high pressure torsion

1. Introduction

Thermoelectric devices can be used either as refrigerators (Peltier effect) or electric power generators (Seebeck effect). Despite their relatively small conversion efficiency, they are commercialized for localized or silent refrigeration and they are considered for powering the wireless sensors required by future applications such as the “Internet of Things” [1] or the “Industry 4.0” [2].

The conversion efficiency of a thermoelectric device (power generator or cooler) is related to the dimensionless figure of merit ZT of its constituting materials. ZT is defined by the expression $ZT = (\alpha^2/\rho)(T/\lambda)$ with α the Seebeck coefficient, ρ the electrical resistivity, λ the thermal conductivity, and T the absolute temperature. Bismuth telluride (Bi₂Te₃), which is the material currently used in commercialized thermoelectric refrigerators, displays a high dimensionless figure of merit $ZT = 1$ at 300 K for both n - & p -type doping. Bismuth and tellurium are indeed chemical elements favorable in several ways to high thermoelectric performances. They often form small-gap semi-conducting compounds with a high electronic mobility, which arises from the non-ionic and strongly covalent character of their chemical bonds. The large atomic mass of these two elements also confer to their compounds a small thermal conductivity. However, the cost of tellurium (~ 150 \$/kg) which arises from its scarcity in the Earth’s crust prevents a broader use of Bi₂Te₃ in applications: a mass-market based on bulk materials incorporating this element is most likely non-sustainable. Cheaper and more abundant thermoelectric materials are thus needed to replace Bi₂Te₃.

Fe₂VAl is the Heusler alloy [3] that could challenge Bi₂Te₃ as a thermoelectric material. Its constituting chemical elements are inexpensive [4] and it displays a power factor equal to $PF = \alpha^2/\rho \sim 5 \text{ mW}\cdot\text{m}^{-1}\cdot\text{K}^{-2}$ at 300 K [5], larger than in Bi₂Te₃. However, Fe₂VAl is not yet a substitute of Bi₂Te₃ because its thermal conductivity is more than one order of magnitude larger ($27 \text{ W}\cdot\text{m}^{-1}\cdot\text{K}^{-1}$ at 300 K in pristine Fe₂VAl) than in Bi₂Te₃, leading to $ZT \sim 0.1$. It is thus mandatory to decrease its thermal conductivity to make it competitive with Bi₂Te₃. The thermal conductivity is the sum of the electronic thermal conductivity (λ_e) and the lattice thermal conductivity (λ_L). Once the power factor has been maximized by controlling the charge carrier concentration, the electronic thermal conductivity which varies like the electrical conductivity (Wiedemann-Franz law) cannot be reduced and only the lattice thermal conductivity can be decreased.

Several research paths have been undertaken in the literature to decrease the lattice thermal conductivity in Fe₂VAl. The first one relies on scattering of heat carrying phonons by the atomic mass fluctuations which arise when one of the constituting element is substituted by a heavier one [6]. A decrease in the lattice thermal conductivity in alloyed Fe₂VAl was first published by Nishino et al. [7] who substituted Al by Si or Ge: it decreased from $\lambda_L = 27 \text{ W}\cdot\text{m}^{-1}\cdot\text{K}^{-1}$ at 300 K in Fe₂VAl to $\lambda_L = 15 \text{ W}\cdot\text{m}^{-1}\cdot\text{K}^{-1}$ in Fe₂VAl_{0.9}Si_{0.1} and $\lambda_L = 11 \text{ W}\cdot\text{m}^{-1}\cdot\text{K}^{-1}$ in Fe₂VAl_{0.9}Ge_{0.1} at 300 K. Since then, many other chemical elements have been substituted and even multi-substituted Fe₂VAl alloys have been investigated [8]. Most of the data reported in the literature on this subject are compiled in Table 1.

Table 1. Compilation of published lattice thermal conductivity values, measured at 300 K in substituted Fe₂VAl alloys.

Composition	$\lambda_L \text{ (W}\cdot\text{m}^{-1}\cdot\text{K}^{-1}\text{)}$	Reference
Fe ₂ VAl	27	[7]
Fe ₂ VAl _{0.9} Si _{0.1}	15	[7]
Fe ₂ VAl _{0.9} Ge _{0.1}	11	[7]
Fe ₂ V _{0.95} Ti _{0.05} Al	25	[9]
Fe ₂ V _{0.95} Nb _{0.05} Al	13	[10]
Fe ₂ V _{0.9} Ti _{0.05} Ta _{0.05} Al	10	[11]
Fe ₂ VAl _{0.95} Ta _{0.05}	7	[12]
Fe ₂ VAl _{0.9} Ta _{0.1}	5	[12]
Fe _{1.9} Re _{0.1} VAl	6	[9]
Fe _{1.9} Co _{0.1} VAl	16.5	[13]
Fe _{1.9} Ni _{0.1} VAl	17	[14]
Fe _{1.9} Ir _{0.1} VAl	5	[15]
Fe ₂ V _{0.95} Ta _{0.05} Al _{0.95} Si _{0.05}	6	[8]
Fe ₂ V _{0.8} Ti _{0.15} W _{0.05} Al	6	[8]

One can easily notice in Table 1 that substitution by one or several heavy elements is an efficient way to decrease λ_L in Fe₂VAl since it leads to a $\sim 80\%$ reduction. Nonetheless, the lowest value of lattice thermal conductivity achieved in substituted Fe₂VAl ($5 \text{ W}\cdot\text{m}^{-1}\cdot\text{K}^{-1}$) is still three times larger than in Bi₂Te₃ ($\sim 1.5 \text{ W}\cdot\text{m}^{-1}\cdot\text{K}^{-1}$). Nanostructuring has been the other research path which was thus implemented to further decrease λ_L and it is the goal of this article to review its effect on the thermoelectric properties of Fe₂VAl.

2. Nanostructured Fe₂VAl

Improved performances were observed in thermoelectric materials with strongly reduced grain sizes [16,17]. In these nanostructured materials, the improvement is related to a decrease in the lattice thermal conductivity promoted by enhanced rates of phonons scattering on the numerous grain boundaries induced by their fine microstructure [18,19]. Reductions of λ_L by 25%, 37%, and 90% at 300 K were for instance observed in *n*-type Half-Heusler ($\sim 200 \text{ nm}$ crystals) [20], in *n*-type filled skutterudites ($\sim 150 \text{ nm}$ crystals) [21] and in silicon ($\sim 20 \text{ nm}$ crystals) [22] respectively. Methods

such as ball milling (BM) combined with Spark Plasma Sintering (SPS), melt spinning (MS), and high pressure torsion (HPT) were thus implemented in alloyed Fe_2VAl , leading to fine-grained samples and to a decrease in the lattice thermal conductivity. Nonetheless, the thermoelectric figure of merit was improved in only very few cases because upon nanostructuring, the electrical resistivity increases as well. In the next sections, a detailed examinations of these results will be presented.

2.1. Synthesis, Microstructure and Thermal Conductivity

Mikami et al. [23] published the first research work on nanostructured $\text{Fe}_2\text{VAl}_{0.9}\text{Si}_{0.1}$. They mechanically alloyed in a planetary ball mill powders of elemental Fe, V, and Si with a Fe-Al alloy [24] and obtained a powder constituted by a face-centered cubic solid solution of these elements. This powder is a collection of micrometric particles ($\sim 7 \mu\text{m}$) which agglomerate much smaller nanocrystallites ($\sim 20 \text{ nm}$). After spark plasma sintering at temperature ranging between 900 and 1000 °C, this solid solution orders in the $L2_1$ structure. The densified samples are polycrystals with an average grain size (D) and a relative density (d) which increase with the sintering temperature and range from $D \sim 100 \text{ nm}$ to $D \sim 400 \text{ nm}$ and $d = 80\%$ to $d = 98\%$ respectively. A scanning electron microscope (SEM) image of the densest sample in Ref. [23] is displayed in Figure 1.

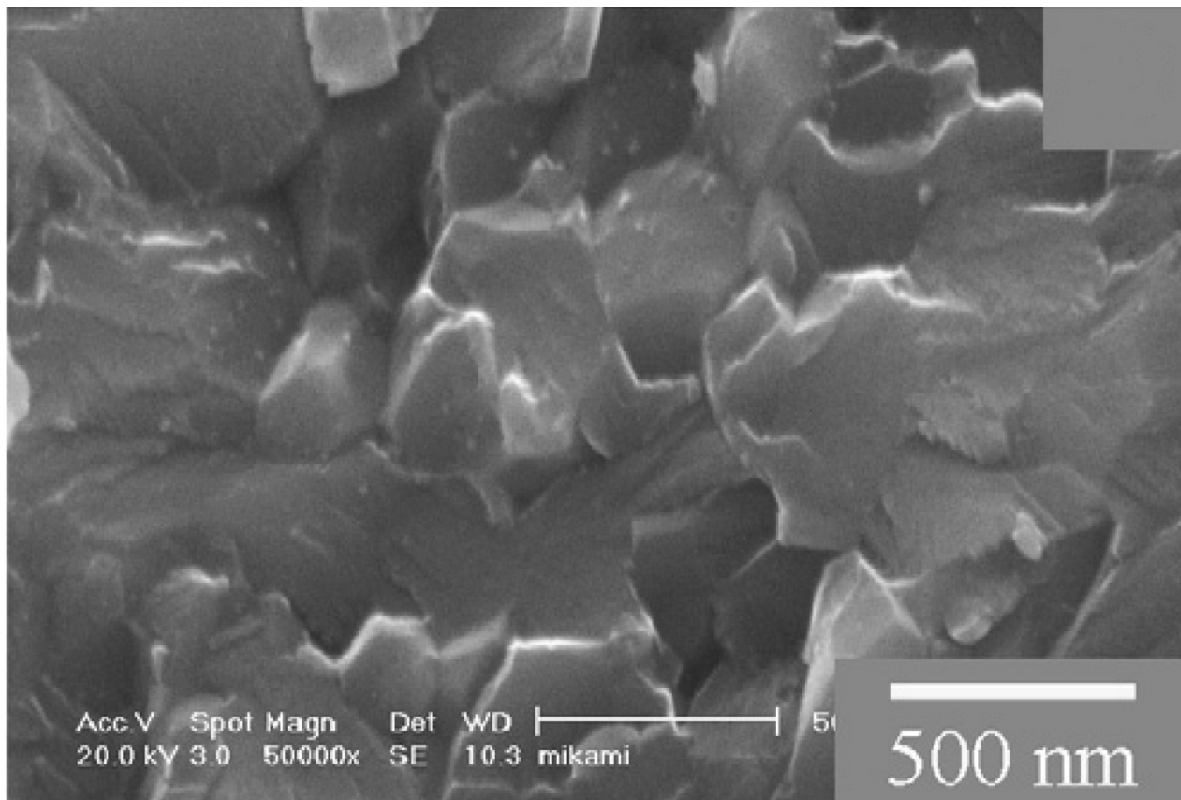


Figure 1. Scanning electron microscope image of mechanically alloyed and sintered (1000 °C) $\text{Fe}_2\text{VAl}_{0.9}\text{Si}_{0.1}$. Reproduced from [23], with copyright permission from Elsevier, 2008.

As expected, upon reduction of the grain size, the thermal conductivity decreases in $\text{Fe}_2\text{VAl}_{0.9}\text{Si}_{0.1}$. It is nonetheless also decreased by the pores which are present in the samples since their relative density is smaller than 100%. In the present review, in order to account of the porosity and to compare values of thermal conductivity only affected by the grain size reduction, the original Mikami's data were corrected by the effective medium theory expression of Odelevski [25]: $\lambda_{real} = \frac{2\lambda_{meas.}}{(3d-1)}$ where λ_{meas} is the measured thermal conductivity, d is the relative density and λ_{real} is the value of a 100% dense sample. For average grain sizes ranging from micron-size (arc-melted sample) to $D \sim 400 \text{ nm}$ and to $D \sim 100 \text{ nm}$,

the lattice thermal conductivity decreases from $\lambda_L = 16.5 \text{ W}\cdot\text{m}^{-1}\cdot\text{K}^{-1}$ to $\lambda_L = 13.4 \text{ W}\cdot\text{m}^{-1}\cdot\text{K}^{-1}$ and to $\lambda_L = 7.9 \text{ W}\cdot\text{m}^{-1}\cdot\text{K}^{-1}$. Given the large uncertainty on the average grain size, it is difficult to use a model like Nan and Birringer's [26] to assess more quantitatively the efficiency of phonon scattering by the grain boundaries. Anyway in Mikami's work, this effect is strong enough to decrease λ_L by 12% when comparing the densest nanostructured $\text{Fe}_2\text{VAl}_{0.9}\text{Si}_{0.1}$ ($d = 98\%$, $D = 400 \text{ nm}$) to the arc-melted (AM) one. Subsequently, by using more energetic conditions at the ball milling stage, a smaller average grain size of $D \sim 300 \text{ nm}$ was achieved in $\text{Fe}_2\text{VAl}_{0.9}\text{Si}_{0.1}$ by Ref. [27]. This led to $\lambda_L = 9.2 \text{ W}\cdot\text{m}^{-1}\cdot\text{K}^{-1}$, a value even smaller which shows directly the effect of grain boundary scattering on thermal transport.

Other compositions than Si-substituted Fe_2VAl were also nanostructured by the same techniques: for instance $\text{Fe}_2\text{VAl}_{0.9}\text{Si}_{0.07}\text{Sb}_{0.03}$ [28] and $\text{Fe}_2\text{V}_{1-y}\text{W}_y\text{Al}$ ($0 \leq y \leq 0.1$) [27] which displayed average grain sizes similar to the previously cited research works, $D \sim 400 \text{ nm}$ and $D \sim 300 \text{ nm}$, respectively. Figure 2 shows the effect on the lattice thermal conductivity of varying the concentration of W in $\text{Fe}_2\text{V}_{1-y}\text{W}_y\text{Al}$ and compares it to $\text{Fe}_2\text{VAl}_{1-x}\text{Si}_x$ ($0 \leq x \leq 0.1$). It can easily be noticed that substituting W, a heavy 5d element, rather than Si leads to an extra $-6 \text{ W}\cdot\text{m}^{-1}\cdot\text{K}^{-1}$ decrease in the lattice thermal conductivity which is equal to $\lambda_L = 3.3 \text{ W}\cdot\text{m}^{-1}\cdot\text{K}^{-1}$ in nanostructured ($D \sim 300 \text{ nm}$ and $d \geq 98\%$) $\text{Fe}_2\text{V}_{0.9}\text{W}_{0.1}\text{Al}$.

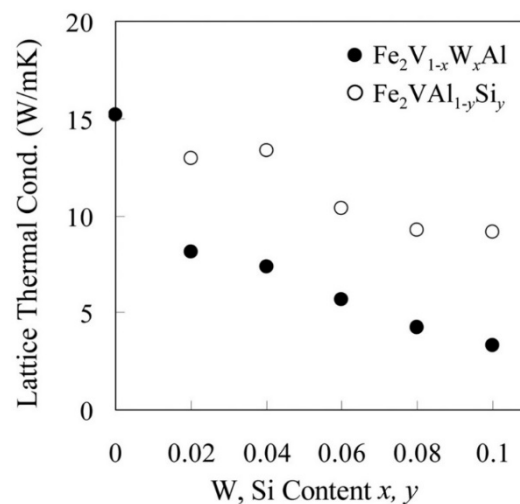


Figure 2. Lattice thermal conductivity at 300 K in nanostructured $\text{Fe}_2\text{V}_{1-y}\text{W}_y\text{Al}$ and $\text{Fe}_2\text{VAl}_{1-x}\text{Si}_x$ as a function of W or Si concentration. Reproduced from [27], with copyright permission from American Institute of Physics, 2012.

Besides ball milling, high pressure torsion (HPT) followed by annealing was the other technique [29] recently implemented by Masuda et al. to refine the microstructure in alloyed Fe_2VAl [30]. $\text{Fe}_2\text{V}_{1.05}\text{Al}_{0.95}$ and $\text{Fe}_2\text{VAl}_{0.95}\text{Ta}_{0.05}$ were the two investigated compositions, which indeed displayed differing properties under these severe deformations. The average grain size in the latter alloy is approximately $D \sim 100 \text{ nm}$, a very small value for well densified Fe_2VAl , whereas it is $D \sim 400 \text{ nm}$ in the former alloy. The authors ascribed this effect to a slowdown of the grain boundary migration by the excess Ta segregated at these grain boundaries. Microstrains have also been previously invoked in HPT-treated skutterudites [31] to act as phonon scatterers and to decrease the thermal conductivity. Nonetheless, the strain due to HPT deformation “almost vanished in $\text{Fe}_2\text{VAl}_{0.95}\text{Ta}_{0.05}$ by annealing at 900 K” [30] and its effect on λ_L can be neglected. Hence, by the combined effect of the grain boundaries and the mass fluctuations arising from the substitution of heavy Ta, the lattice thermal conductivity is decreased to $\lambda_L = 3.2 \text{ W}\cdot\text{m}^{-1}\cdot\text{K}^{-1}$, a value nearly 10 times smaller than in pristine Fe_2VAl .

Finally, grain boundaries are not the only interface which can scatter phonons: antiphase boundaries separating antiphase domain have newly been shown to decrease the lattice thermal conductivity in Fe_2VAl [32]. Rapidly quenching Fe_2VAl from temperatures where its disordered B2

or A2 variants are stable, allowed stabilizing a nanostructured variant of Fe_2VAl . It is constituted by $L2_1$ antiphase domains (APDs) separated by antiphase boundaries (APBs), which indeed scatter the phonons. When domains as small as ~ 100 nm are synthesized, the lattice thermal conductivity is decreased from 28 to $17 \text{ W}\cdot\text{m}^{-1}\cdot\text{K}^{-1}$ [32].

2.2. Electronic Transport Properties and ZT

In all the previously cited references [23,27,28,30], despite differing compositions, the Seebeck coefficient peaks as a function of temperature (200–500 K) at the same value, e.g., $\sim -130 \mu\text{V}\cdot\text{K}^{-1}$. This is due to the well-established fact that the Seebeck coefficient in most cases does not depend on the exact nature of the dopant but depends on the charge carrier concentrations. Since this last parameter is weakly affected by the modifications of the microstructure, the Seebeck coefficient is also hardly modified and it does not influence the figure of merit.

But the electrical resistivity is not immune to the changes of microstructure because grain boundaries also scatter electrons. In all the previously cited references, as can be noticed in Table 2 when comparing to arc melted samples displaying micrometric grain sizes, resistivity systematically increases when the grain sizes decreases. This compensates the reduction of lattice thermal conductivity previously discussed and hence ZT only marginally increases when the grain size is decreased to $D \sim 400$ nm. In an attempt to circumvent this effect, Mikami et al. synthesized $\text{Fe}_2\text{VAl}_{0.9}\text{Si}_{0.1} + \text{Bi}$ nanocomposites but they did not improve ZT [33]. As can be seen in Figure 3, it is only very recently that, in severely deformed (HPT) and annealed $\text{Fe}_2\text{VAl}_{0.95}\text{Ta}_{0.05}$, the strong decrease in λ_L arising from the very small $D \sim 100$ nm grain size overcomes the increase in electrical resistivity and leads to the improved value of figure of merit $ZT = 0.3$ (+50%) at 500 K. This last example shows that nanostructuring is a promising research path, which leads to improvements of ZT in alloyed Fe_2VAl and that it deserves to be pursued in the next future.

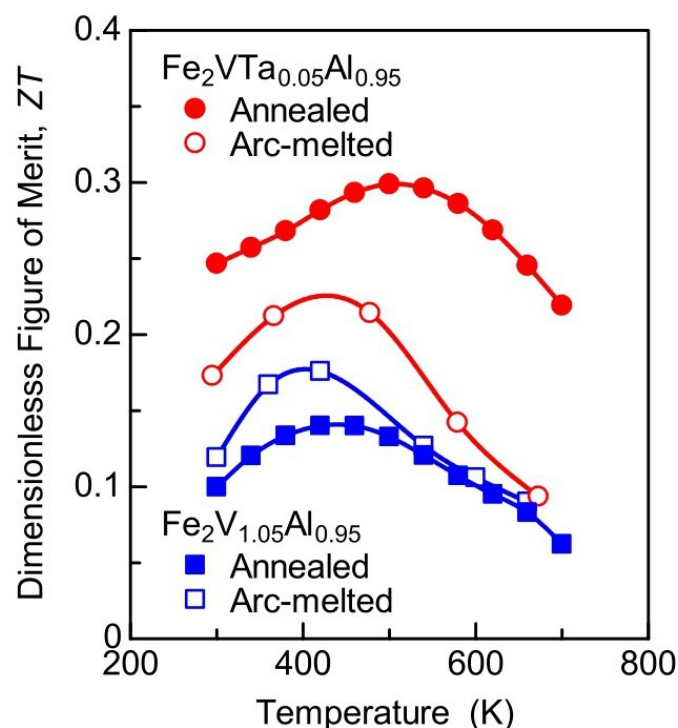


Figure 3. Dimensionless thermoelectric figure of merit as a function of temperature in $\text{Fe}_2\text{V}_{1.05}\text{Al}_{0.95}$ and in $\text{Fe}_2\text{VAl}_{0.95}\text{Ta}_{0.05}$. “Annealed” means severely deformed by HPT, followed by annealing. Reproduced from [30], with copyright permission from American Institute of Physics, 2012.

Table 2. Average grain size (D), thermal, and electronic transport properties in various nanostructured and substituted Fe₂VAI alloys at 300 K except ZT_{max} which is the maximum value of the dimensionless thermoelectric figure of merit as a function of temperature. “AM” stands for arc melted.

Composition	D (nm)	λ_L (W·m ⁻¹ ·K ⁻¹)	λ (W·m ⁻¹ ·K ⁻¹)	ρ (μΩ·m)	ZT_{max}	Reference
Fe ₂ VAI _{0.9} Si _{0.1}	AM	15	18	2.5	0.10	[7]
Fe ₂ VAI _{0.9} Si _{0.1}	~400	13.2	14.8	4.7	0.08	[23]
Fe ₂ VAI _{0.9} Si _{0.1}	~300	9.2	11	4.1	0.12	[27]
Fe ₂ VAI _{0.9} Sb _{0.03} Si _{0.07}	~400	7.4	10.2	2.7	0.15	[28]
Fe ₂ V _{1.05} Al _{0.95}	AM	12.7	15.5	2.6	0.18	[30]
Fe ₂ V _{1.05} Al _{0.95}	~400	10.3	12.5	3.4	0.14	[30]
Fe ₂ VAI _{0.95} Ta _{0.05}	AM	7	9.5	3.0	0.21	[12]
Fe ₂ V _{0.9} W _{0.1} Al	~300	3.3	5	4.5	0.20	[27]
Fe ₂ VAI _{0.95} Ta _{0.05}	~100	3.2	5	4.1	0.30	[30]

3. Conclusions

Ball milling or high pressure torsion lead to nanometric grain size in alloyed Fe₂VAI. The heat carrying phonons are not only scattered by the mass fluctuations provided by alloying but also by the numerous grain boundaries introduced in the microstructure. The lattice thermal conductivity is thus strongly decreased but in most of the reviewed cases, the electrical resistivity is also increased by the refined microstructure and this precludes any gain of ZT . Nonetheless, in severely deformed Fe₂VAI_{0.95}Ta_{0.05} with $D \sim 100$ nm [30], the strong decrease in the lattice thermal conductivity overcompensate the electrical resistivity increase and an improved $ZT = 0.3$ is reached at 500 K. These promising results will certainly be followed by similar research effort to improve ZT by nanostructuring Fe₂VAI.

Conflicts of Interest: The author declares no conflict of interest.

References

1. Wikipedia. Internet of Things. Available online: <https://en.wikipedia.org/wiki/Internetofthings> (accessed on 18 October 2018).
2. Wikipedia. Industry 4.0. Available online: https://en.wikipedia.org/wiki/Industry_4.0 (accessed on 18 October 2018).
3. Felser, C.; Hirohata, A. *Heusler Alloys*; Springer: Cham, Switzerland, 2016; Volume 222.
4. Ferrovandium Price. Available online: <https://minerals.usgs.gov/minerals/pubs/commodity/vanadium/mcs-2018-vanad.pdf> (accessed on 18 October 2018).
5. Kato, H.; Kato, M.; Nishino, Y.; Mizutani, U.; Asano, S. Effect of Silicon Substitution on Thermoelectric Properties of Heusler-type Fe₂VAI Alloy. *Jpn. Inst. Met.* **2001**, *65*, 652–656. [CrossRef]
6. Bhandari, C.M. Minimizing the Thermal Conductivity. In *CRC Handbook of Thermoelectrics*; Rowe, D.M., Ed.; CRC Press: Boca Raton, FL, USA, 1995.
7. Nishino, Y.; Deguchi, S.; Mizutani, U. Thermal and transport properties of the Heusler-type Fe₂VAI_{1-x}Ge_x (0 < x < 0.20) alloys: Effect of doping on lattice thermal conductivity, electrical resistivity, and Seebeck coefficient. *Phys. Rev. B* **2006**, *74*, 115115.
8. Takeuchi, T.; Terazawa, Y.; Furuta, Y.; Yamamoto, A.; Mikami, M. Effect of Heavy Element Substitution and Off-Stoichiometric Composition on Thermoelectric Properties of Fe₂VAI-Based Heusler Phase. *J. Electron. Mater.* **2013**, *42*, 2084–2090. [CrossRef]
9. Kobayashi, F.; Ide, N.; Nishino, Y. Effects of Re Substitution on Thermoelectric Properties of Pseudogap System Fe₂VAI. *Jpn. Inst. Met.* **2007**, *71*, 208–212. [CrossRef]
10. Kurosaki, K.; Muta, H.; Endo, Y.; Charoenphakdee, A.; Uno, M.; Yamanaka, S. Effect of Nb substitution for V on the thermoelectric properties of Fe₂VAI. *J. Alloys Compd.* **2009**, *486*, 507–510. [CrossRef]
11. Mori, T.; Ide, N.; Nishino, Y. Thermoelectric Properties of p-Type Fe₂V_{1-x-y}Ti_xTa_yAl Alloys. *Jpn. Inst. Met.* **2008**, *72*, 593–598. [CrossRef]
12. Renard, K.; Mori, A.; Yamada, Y.; Tanaka, S.; Miyazaki, H.; Nishino, Y. Thermoelectric properties of the Heusler-type Fe₂VTa_xAl_{1-x} alloys. *J. Appl. Phys.* **2014**, *115*, 033707. [CrossRef]

13. Lu, W.; Zhang, W.; Chen, L. Thermoelectric properties of $(\text{Fe}_{1-x}\text{Co}_x)_2\text{VAl}$ Heusler-type compounds. *J. Alloys Compd.* **2009**, *484*, 812–815. [[CrossRef](#)]
14. Knapp, I.; Budinska, B.; Milosavljevic, D.; Heinrich, P.; Khmelevskiy, S.; Moser, R.; Podloucky, R.; Prenninger, P.; Bauer, E. Impurity band effects on transport and thermoelectric properties of $\text{Fe}_{2-x}\text{Ni}_x\text{VAl}$. *Phys. Rev. B* **2017**, *96*, 045204. [[CrossRef](#)]
15. Sugiura, T.; Nishino, Y. Doping Effects of Transition Metals on Thermoelectric Properties of Off-Stoichiometric Fe_2VAl Alloys. *J. Jpn. Inst. Met.* **2009**, *73*, 846–851. [[CrossRef](#)]
16. Poudel, B.; Hao, Q.; Ma, Y.; Lan, Y.; Minnich, A.; Yu, B.; Yan, X.; Wang, D.; Muto, A.; Vashace, D.; et al. High thermoelectric performance of nanostructured bismuth antimony telluride bulk alloys. *Science* **2008**, *320*, 634–638. [[CrossRef](#)] [[PubMed](#)]
17. Joshi, G.; Lee, H.; Lan, Y.; Wang, X.; Zhu, G.; Wang, D.; Gould, R.W.; Cuff, D.C.; Tang, M.Y.; Dresselhaus, M.S.; et al. Enhanced Thermoelectric Figure-of-Merit in Nanostructured p-type Silicon Germanium Bulk Alloys. *Nano Lett.* **2008**, *8*, 4670–4674. [[CrossRef](#)] [[PubMed](#)]
18. Minnich, A.J.; Dresselhaus, M.S.; Ren, Z.F.; Chen, G. Bulk nanostructured thermoelectric materials: Current research and future prospects. *Energy Environ. Sci.* **2009**, *2*, 466–479. [[CrossRef](#)]
19. Vineis, C.J.; Shakouri, A.; Majumdar, A.; Kanatzidis, M.G. Nanostructured Thermoelectrics: Big Efficiency Gains from Small Features. *Adv. Mater.* **2010**, *22*, 3970–3980. [[CrossRef](#)] [[PubMed](#)]
20. Joshi, G.; Yan, X.; Wang, H.; Liu, W.; Chen, G.; Ren, Z. Enhancement in Thermoelectric Figure-of-Merit of an N-Type Half-Heusler Compound by the Nanocomposite Approach. *Adv. Energy Mater.* **2011**, *1*, 643–647. [[CrossRef](#)]
21. Benyahia, M.; Ohorodniichuk, V.; Leroy, E.; Dauscher, A.; Lenoir, B.; Alleno, E. High thermoelectric figure of merit in mesostructured $\text{In}_{0.25}\text{Co}_4\text{Sb}_{12}$ n-type skutterudite. *J. Alloys Compd.* **2018**, *735*, 1096–1104. [[CrossRef](#)]
22. Bux, S.K.; Blair, R.G.; Gogna, P.K.; Lee, H.; Chen, G.; Dresselhaus, M.S.; Kaner, R.B.; Fleurial, J.P. Nanostructured Bulk Silicon as an Effective Thermoelectric Material. *Adv. Funct. Mater.* **2009**, *19*, 2445–2452. [[CrossRef](#)]
23. Mikami, M.; Matsumoto, A.; Kobayashi, K. Synthesis and thermoelectric properties of microstructural Heusler Fe_2VAl alloy. *J. Alloys Compd.* **2008**, *461*, 423–426. [[CrossRef](#)]
24. Kamiya, N.; Ozaki, K.; Kobayashi, K.; Ozaki, K.; Mikami, H. Heusler iron-Based Thermoelectric Powder and Manufacture of Heusler Iron-Based Thermoelectric Material. Patent No. JP2011233797A, 17 November 2011.
25. Odelevskii, V.I. Calculation of general conductivity of heterogeneous systems II. Random mixtures of non-elongated particles. *J. Tech. Phys.* **1951**, *21*, 678–685.
26. Nan, C.-W.; Birringer, R. Determining the Kapitza resistance and the thermal conductivity of polycrystals: A simple model. *Phys. Rev. B* **1998**, *57*, 8264–8268. [[CrossRef](#)]
27. Mikami, M.; Kinemuchi, Y.; Ozaki, K.; Terazawa, Y.; Takeuchi, T. Thermoelectric properties of tungsten-substituted Heusler Fe_2VAl alloy. *J. Appl. Phys.* **2012**, *111*, 093710. [[CrossRef](#)]
28. Mikami, M.; Tanaka, S.; Kobayashi, K. Thermoelectric properties of Sb-doped Heusler Fe_2VAl alloy. *J. Alloys Compd.* **2009**, *484*, 444–448. [[CrossRef](#)]
29. Zhilyaev, A.P.; Langdon, T.G. Using high-pressure torsion for metal processing: Fundamentals and applications. *Prog. Mater. Sci.* **2008**, *53*, 893–979. [[CrossRef](#)]
30. Masuda, S.; Tsuchiya, K.; Qiang, J.; Miyazaki, H.; Nishino, Y. Effect of high-pressure torsion on the microstructure and thermoelectric properties of Fe_2VAl -based compounds. *J. Appl. Phys.* **2018**, *124*. [[CrossRef](#)]
31. Zhang, L.; Grytsiv, A.; Bonarski, B.; Kerber, M.; Setman, D.; Schafler, E.; Rogl, P.; Bauer, E.; Hilscher, G.; Zehetbauer, M. Impact of high pressure torsion on the microstructure and physical properties of $\text{Pr}_{0.67}\text{Fe}_3\text{CoSb}_{12}$, $\text{Pr}_{0.71}\text{Fe}_{3.5}\text{Ni}_{0.5}\text{Sb}_{12}$, and $\text{Ba}_{0.06}\text{Co}_4\text{Sb}_{12}$. *J. Alloys Compd.* **2010**, *494*, 78–83. [[CrossRef](#)]
32. Maier, S.; Perrière, L.; Bourgon, J.; Leroy, E.; Beaudhuin, M.; Alleno, E. Phonon scattering by antiphase boundaries in the Fe_2VAl Heusler alloy. 2018; under review.
33. Mikami, M.; Kobayashi, K. Effect of Bi addition on microstructure and thermoelectric properties of Heusler Fe_2VAl sintered alloy. *J. Alloys Compd.* **2008**, *466*, 530–534. [[CrossRef](#)]

